

Structural and photophysical properties of hydroxyapatite doped with lanthanide ions

Propriedades estruturais e fotofísicas da hidroxiapatita dopada com íons lantanídeos

Amanda Alves Barbosa^{1,2}, Severino Alves Junior¹,
Raquel Aline Pessoa Oliveira², Andréa de Vasconcelos Ferraz²

¹ Universidade Federal de Pernambuco - Av. Jorn. Aníbal Fernandes, s/nº, Cidade Universitária, Recife, PE, Brasil.

² Universidade Federal do Vale do São Francisco - Av. Antonio Carlos Magalhaes 310, Juazeiro, BA, Brasil.

e-mail: amanda.barbosa@univasf.edu.br, salvesjr@ufpe.br, raquel.oliveira@univasf.edu.br, andrea.ferraz@univasf.edu.br.

RESUMO

Matrizes de hidroxiapatita (HAp) dopadas com os íons lantanídeos Eu^{3+} , Ce^{3+} e Gd^{3+} , $[\text{Ca}_{10-x}\text{Ln}_x(\text{PO}_4)_6(\text{OH})_2]$, foram obtidas pelo método da precipitação com o objetivo de estudar suas propriedades fotofísicas. A partir de análises de Microscopia Eletrônica de Varredura observou-se que amostras dopadas com íons lantanídeos (Ln^{3+}) apresentaram similaridade com a morfologia da HAp pura, por outro lado nos difratogramas de Raios X a partir do refinamento Rietveld verificou-se que a matriz aparece como fase majoritária ($\approx 70\%$) enquanto ($\approx 30\%$) de uma fase secundária de tricálcio fosfato (TCP) foi conferida em função das diferentes dopagens. Isotermas de adsorção obtidas pela técnica BET indicaram que todos os materiais sintetizados são classificados como mesoporosos. Os espectros de emissão dos materiais exibem bandas características dos íons Ln^{3+} incorporados à estrutura da matriz em 573 nm (${}^5\text{D}_0 \rightarrow \text{F}_0$), 600 nm (${}^5\text{D}_0 \rightarrow \text{F}_1$), 628 nm (${}^5\text{D}_0 \rightarrow \text{F}_2$), e 698 nm (${}^5\text{D}_0 \rightarrow \text{F}_4$) para HAp/Eu, 337-360 nm (5d \rightarrow 4f) para HAp/Ce e em 425 nm para HAp/Gd.

Palavras-chave: Hidroxiapatita; Compósito; Luminescente; Biomaterial; Propriedades.

ABSTRACT

Hydroxyapatite (HAp) matrices doped with lanthanide ions Eu^{3+} , Ce^{3+} and Gd^{3+} , $[\text{Ca}_{10-x}\text{Ln}_x(\text{PO}_4)_6(\text{OH})_2]$ were obtained through the precipitation method so their photophysical properties could be studied. From the Scanning Electron Microscopy analyzes it was observed that samples doped with lanthanide ions (Ln^{3+}) showed similarity with the morphology of pure HAp, whereas Rietveld-refined X-ray diffractograms showed that the matrix appears as the major phase ($\approx 70\%$) while ($\approx 30\%$) of a second phase of tricalcium phosphate (TCP) was due to the different doping levels. Adsorption isotherms obtained by the BET technique indicated that all the synthesized materials are classified as mesoporous. The emission spectra of the materials exhibit bands typical of the Ln^{3+} ions incorporated into the matrix structure at 573 nm (${}^5\text{D}_0 \rightarrow \text{F}_0$), 600 nm (${}^5\text{D}_0 \rightarrow \text{F}_1$), 628 nm (${}^5\text{D}_0 \rightarrow \text{F}_2$), and 698 nm (${}^5\text{D}_0 \rightarrow \text{F}_4$) for HAp/Eu, 337-360 nm (5d \rightarrow 4f) for HAp/Ce and at 425 nm for HAp/Gd.

Keywords: Hydroxyapatite; Composite; Luminescent; Biomaterial; Properties.

1. INTRODUCTION

The mineral apatite, $\text{Ca}_5(\text{PO}_4)_3\text{X}_2$ (X=F, OH, Cl), is the most abundant natural phosphate on Earth. Its chemical structure contains many replacements between cations and anions - practically half of the periodic table can be incorporated to its atomic arrangement, which is one of the most interesting properties of apatites [1]. In biological systems, the apatite variety called hydroxyapatite, $\text{Ca}_{10}(\text{PO}_4)_6(\text{OH})_2$, consists of the major mineral component of bones and teeth [2]. Because of its high chemical and crystallographic similarity to the

bone structure, synthetic HAp is considered a bioactive substance, since it binds strongly to the host bone tissue. In addition, it is a biocompatible, osteoconductive, non-immunogenic and non-toxic material [3]. These characteristics make HAp a suitable biomaterial for medical applications, with it being widely used as bone grafts and highly promising for clinical use [3].

The replaced apatites are generally produced by synthesis; in the case of HAp, different routes are used in their production such as the reaction sol-gel [4, 5], microwave irradiation [6, 7] and precipitation reaction [8, 9], the latter being the most used. The ease of performing ionic exchanges in the HAp structure can be attributed to its broad surface area, besides the existence of a metastable hydrate layer on the surface of the nanocrystals whose ionic bonds are weak [10, 11].

Considering the characteristics presented by HAp as a good host material, the introduction of trivalent lanthanide ions (Ln^{3+}), due to its optical properties and great applicability, has aroused the interest of several research groups. ZENG *et al.* [12] developed a polymeric biosensor doped with Ce^{3+} and Tb^{3+} ions capable of detecting H_2O_2 , indicating potential for use in the determination of glucose. CANTARELLI *et al.* [13] proposed the incorporation of Gd^{3+} , Yb^{3+} , Er^{3+} and Gd^{3+} , Yb^{3+} , Tm^{3+} ions in CaF_2 nanoparticles producing biocompatible nanoprobe for biomedical images, which were efficient for surgical applications. In our research group, various studies involving the spectroscopic study of materials containing lanthanide ions have already been developed, such as SOUZA *et al.* [14]. The authors carried out the doping of a polymer with Eu (III) and Tb (III) complexes and obtained red and green solid state emitters. LIMA *et al.* [15] synthesized complexes of lanthanide ions (Eu^{3+} , Tb^{3+} and Gd^{3+}) with ligands derived from dicarboxylic acids to study the effect of the substituents on the luminescence of lanthanide ions in the Eu^{3+} and Tb^{3+} complexes.

Thus, the objective of the present work was to evaluate the incorporation of different Ln^{3+} ions into an inorganic matrix (HAp) and to study its photophysical properties for the development of a luminescent biomaterial with potential for application in the medical field.

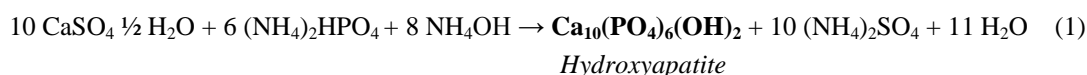
2. MATERIALS AND METHODS

2.1 Materials

The following analytical grade chemical reagents were used in the synthesis of doped HAp: $(\text{NH}_4)_2\text{HPO}_4$ (Vetec), NH_4OH (Scientific Exodus), HCl (Vetec), Eu_2O_3 , Gd_2O_3 and Ce_2O_3 (Sigma-Aldrich). The source of calcium used was gypsum β , $\text{CaSO}_4 \cdot \frac{1}{2}\text{H}_2\text{O}$, with a 80-95% purity, provided by Industrial Mineral Gypsum Ltda.

2.2 Synthesis of the Hydroxyapatite Matrix

Hydroxyapatite was obtained by the precipitation method [16], with a molar ratio of 1.66 Ca/P, according to the reaction represented by equation (1).



Initially, 250 mL of a 0.1 mol.L⁻¹ $\text{CaSO}_4 \cdot \frac{1}{2}\text{H}_2\text{O}$ solution was placed under stirring and then a 3.0 mol.L⁻¹ NH_4OH solution was added until pH = 10. Subsequently, 250 mL of a 0.06 mol.L⁻¹ $(\text{NH}_4)_2\text{HPO}_4$ solution was added at a flow rate of 20 mL.min⁻¹. The pH was maintained around 10 through the addition of 3.0 mol.L⁻¹ NH_4OH until the end of the synthesis. After the addition of all reagents, the system remained under magnetic stirring for one hour for complete homogenization of the mixture. Then, the system stood still for the sedimentation of the denser component. The material produced was vacuum-filtered and washed with deionized water until neutral pH and then oven-dried at 100 °C for 24 hours. The dried material was triturated and then calcined at 900 °C for 2 hours with a heating rate of 10 °C.min⁻¹.

2.3 Synthesis of the Doped Hydroxyapatite Matrix with Lanthanide ions

The process of synthesis of the HAp doped with lanthanide ions followed the same methodology used in the preparation of pure HAp. For each of the doped materials, HAp/Eu, HAp/Ce and HAp/Gd, 2.0 % of the molar amount of Ca^{2+} ions was replaced by the respective Ln^{3+} ion in the form of chlorides. The addition was made during the stirring step of calcium sulphate, following the same procedures described in item 2.1.2.

2.4 Characterizations

The synthesized materials were characterized by several techniques, such as Scanning Electron Microscopy with X-ray Dispersive Energy Analysis (Hitachi TM1000 and Vega 3 Tescan) used to observe the sample morphology. The structure of the materials was characterized by infrared spectra obtained by FTIR equipment, Model: Spectrum Two, in the range of 4000-400 cm^{-1} wave numbers. Samples were prepared as KBr pellets using mechanical pressing.

The analysis of the crystalline phases was done by X-ray diffraction (XRD) with the Difract ACT 1000 series (Siemens), using the copper $k\alpha$ line ($\lambda = 1.54056 \text{ \AA}$) at 40 kV and 40 mA. The 2θ range was 20° to 50° , with a step of 0.02° and integration time of 1s per point. Phase identification was confirmed using the Rietveld method employed X'Pert HighScore Plus software version 2.0a. The experimental XRD pattern was compared to the parameters of ICSD 16742 reference sheets corresponding to HAp ($\text{Ca}_{10}(\text{PO}_4)_6(\text{OH})_2$), belonging to the hexagonal crystal system, and to the spatial group P63/ m. The crystallographic parameters were: $a = 9.4320 \text{ \AA}$, $b = 9.4320 \text{ \AA}$, $c = 6.8810 \text{ \AA}$, $\alpha = 90^\circ$, $\beta = 90^\circ$ and $\gamma = 120^\circ$ and ICSD 6191 corresponds to Tricalcium Phosphate (TCP) ($\text{Ca}_3(\text{PO}_4)_2$), belonging to the rhombohedral crystal system, and the space group R3c. The crystallographic parameters were: $a = 10.4390 \text{ \AA}$, $b = 10.4390 \text{ \AA}$, $c = 37.3750 \text{ \AA}$, $\alpha = 90^\circ$, $\beta = 90^\circ$ and $\gamma = 120^\circ$.

The Brunauer-Emmett-Teller (BET) surface area measurements were performed by the Micrometrics ASAP 2420 surface area analyzer. The photoluminescent properties of the solid-state materials were investigated in a Jobin-Yvon Ramanor U-1000 double-monochromator spectrofluorometer. For excitation, a Jobin-Yvon monochromator model H-10 was used, using a Xe-Hg lamp (150W).

3. RESULTS AND DISCUSSION

The FTIR spectra for both pure HAp and HAp doped with the different lanthanide ions are shown in Figure 1. As observed, HAp/Eu, HAp/Ce and HAp/Gd have the same spectral profiles. Vibrations of 569 to 609 cm^{-1} are attributed to O-P-O (ν_4) deformation in PO_4^{3-} or angular deformation O-P-O (ν_4) in HPO_4^{2-} ; 954 to 956 cm^{-1} for symmetrical stretching P-O (ν_1) of the PO_4^{3-} group; 1032 to 1100 cm^{-1} for asymmetric stretching of PO_4^{3-} (ν_3) or stretching PO_3 (ν_6) in HPO_4^{2-} ; low intensity bands were verified at 1630 to 1633 cm^{-1} corresponding to the deformation H-O-H indicating the presence of H_2O ; 636 to 643 cm^{-1} are OH⁻ hydroxyl vibrations and 3575 to 3579 cm^{-1} for hydroxyl OH⁻ (ν_5) stretching, in accordance with the standards verified by YANG *et al.* [17].

The presence of OH⁻ groups found in the samples indicates that HAp has binding sites suitable for incorporation of drug molecules; therefore, the material presents an important property for its use as a support for drugs [18].

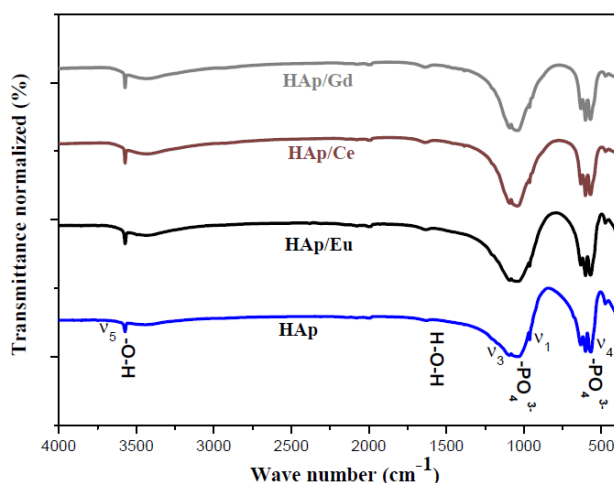


Figure 1: FTIR spectra of the materials HAp, HAp/Eu, HAp/Ce and HAp/Gd.

Figure 2 shows the powder XRD pattern obtained for the samples: HAp/Eu, HAp/Gd and HAp/Ce, where it can be seen that HAp is the major phase; however, the incorporation of lanthanide ions into the matrix structure caused the appearance of a peak at $2\theta = 31.0^\circ$ attributed to phosphate tricalcium phase (TCP). It was verified that the appearance of this phase can be explained by the introduction of the Ln^{3+} ions in the HAp lattice, which occurs by replacing the Ca^{2+} ions in two different crystallographic sites of the unit cell, turning it into $\text{Ca}_{10-x}\text{Ln}_x(\text{PO}_4)_6(\text{OH})_2$, [19] as shown in Figure 3.

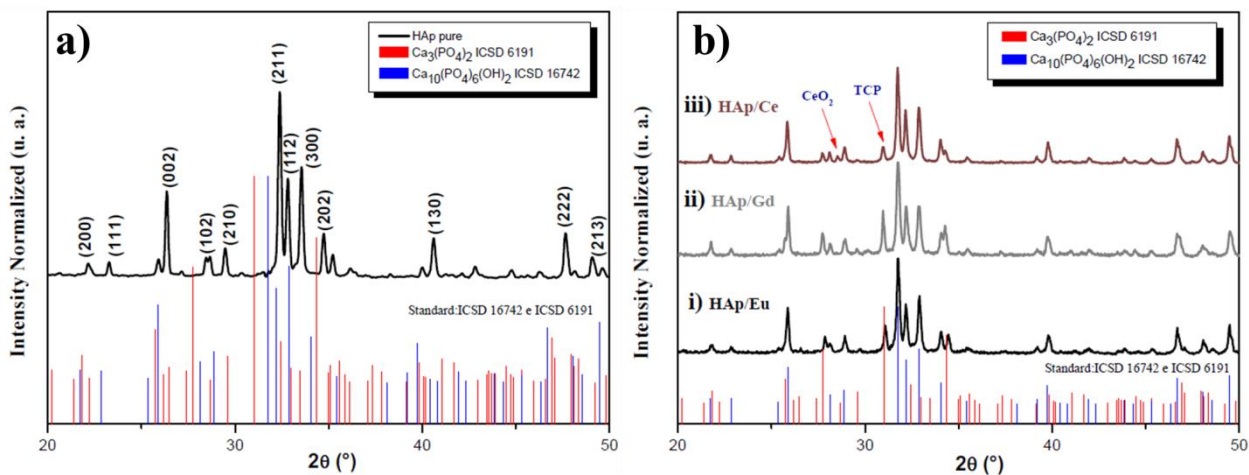


Figure 2: Experimental X ray powder diffraction patterns of a) HAp pure and b) (i) HAp/Eu, (ii) HAp/Gd, (iii) HAp/Ce and standards of reference sheets ICSD 16742 (HAp), ICSD 6191 (TCP).

The unit cell of HAp in the hexagonal phase has 10 calcium ions at two different non-equivalent crystallographic sites. Of these, four ions are at site I (Ca1) and another six located at site II (Ca2). The incorporation of the Ln³⁺ ions: Eu³⁺, Ce³⁺ and Gd³⁺ into the HAp structure of can occur through the occupation of both sites [21], Figure 3-b.

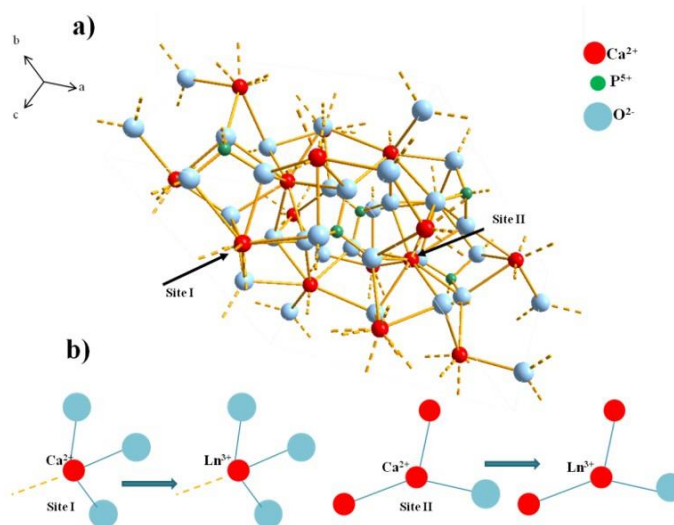


Figure 3: a) Representation of the two different cationic sites occupied by the Ca²⁺ ions in the hydroxyapatite and b) Substitution of the Ln³⁺ ions at the respective Ca²⁺ sites. Crystalline HAp cell obtained with X'Pert HighScore Plus software version 2.0a.

The mechanism of charge compensation for the substitution of Ca²⁺ by Ln³⁺ in the HAp molecule in addition to the heat treatment can result in destabilization of the structure and formation of the TCP phase [22]. The presence of a second phase in the HAp causes an increase in its rate of degradation, and may be an important characteristic for its application in the medical field [23].

In the HAp/Ce diffractogram, a peak observed in 2θ = 28.5° was not compatible with HAp and also did not appear for HAp/Eu and HAp/Gd. From the Rietveld refinement data, it was possible to identify the peak attributed to cerium oxide (CeO₂), indicating that Ce³⁺ ions were not thoroughly incorporated into the matrix structure. Comparing the ionic radii of Ca²⁺ to those of the dopants, Ca²⁺ = 0.106 nm, Eu³⁺ = 0.098 nm, Ce³⁺ = 0.107 nm and Gd³⁺ = 0.097 nm [24], it is observed that Eu³⁺ and Gd³⁺ occupy the vacancies generated by the Ca²⁺ ions more easily because their radii are smaller. On the other hand, the ionic radius of Ce³⁺ is very close, but higher than that of Ca²⁺, and may limit its incorporation into the HAp lattice. MORAIS *et al.* [25] identified characteristic peaks for crystalline cerium oxide in the same region for the sample of HAp

doped with the ion, confirming the results obtained in the diffractogram of Figure 2-b (iii). The influence of the dopants on the appearance of TCP in the material was proven by the quantification of the phases present for each of the samples. According to Table 01, that the values of HAp/Eu and HAp/Gd are very close to the TCP phase, whereas HAp/Ce presents a considerably lower value, demonstrating the complete non-incorporation of the Ce^{3+} ions into the HAp lattice.

Table 1: Percentage of phases depending on the different doping of the material.

SAMPLE	PHASES (%MASS)	
	HAP	TCP
HAp/Eu	64.40	35.60
HAp/Ce	90.87	9.13
HAp/Gd	70.33	29.67

Micrographs of pure HAp are shown in Figure 4, where particles with round shapes and uniform distribution are observed for the non-calcined material, Figure 4-a. For the calcined HAp, the morphology shows changes as a function of the heat treatment; in this case, the particles start a mass diffusion process, causing their size to increase and a change in their shape due to grain growth [9]. GYORGY *et al.* [26] and KAMALATHAN *et al.* [27] observed the densification of HAp powders due to the growth of grains attributed to the diffusion of the particles as a function of the sintering temperature.

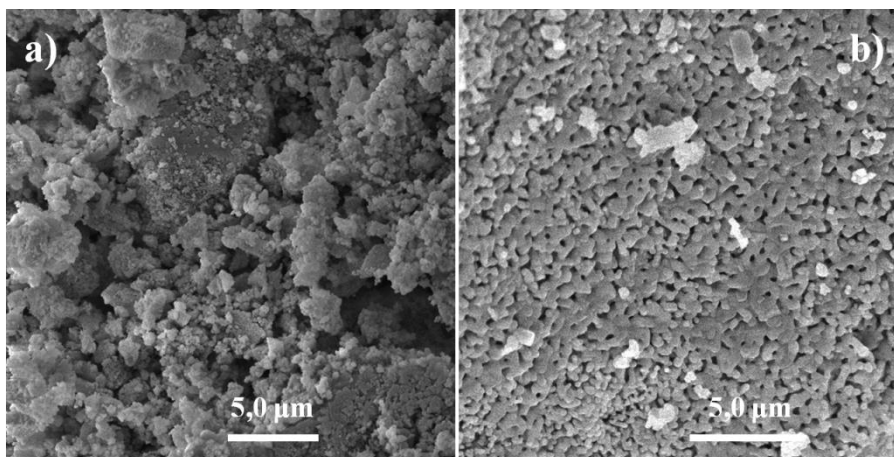


Figure 4: SEM micrographs of samples of HAp pure (a) not calcined and (b) after calcination.

In Figure 5, micrographs of the samples of HAp doped with Ln^{3+} ions are observed. The images of the samples doping with Eu^{3+} and Ce^{3+} , (Figures 5-a and 5-c) show similarity between their morphologies and that observed for the matrix. However, spherical particle clusters were observed for the HAp/Gd sample, Figure 5-e. Also shown in Figure 5 are the EDS spectra for the various samples. In addition to the identification of the main elements that compose HAp as calcium (Ca) and phosphorus (P), doping is confirmed from the low intensity peaks attributed to Ln^{3+} ions: Eu^{3+} , Ce^{3+} e Gd^{3+} incorporated into the HAp structure. The carbon-associated peak is due to the carbon tape used to fix the sample to the sample holder.

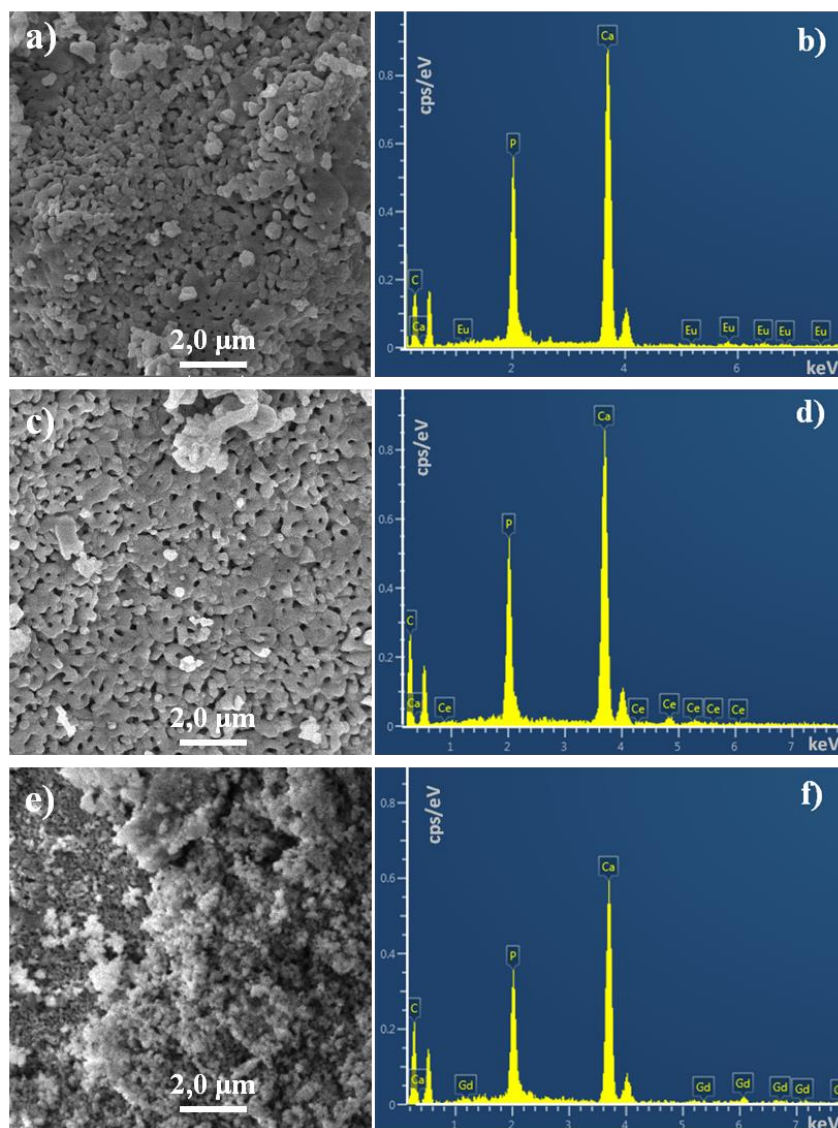


Figure 5: Micrographs obtained by scanning electron microscopy of the matrices of HAp doped with Eu^{3+} , Ce^{3+} and Gd^{3+} ions and their respective dispersive energy spectra: a) and b) HAp/Eu, c) and d) HAp/Ce, e) and f) HAp/Gd.

The adsorption isotherms of pure and doped HAp are shown in Figure 6. According to the IUPAC classification, these curves can be identified as type IV isotherms, which is characterized as a mesoporous material, that is, it has pores with a diameter between 2 and 50 nm [28]. With regard the surface areas BET (S_{BET}) obtained for all samples, it was verified that the Eu^{3+} and Gd^{3+} ions caused a great reduction in S_{BET} (HAp/Eu: $S_{\text{BET}} = 41.44 \text{ m}^2 \cdot \text{g}^{-1}$ and HAp/Gd: $S_{\text{BET}} = 37.95 \text{ m}^2 \cdot \text{g}^{-1}$) when compared to pure material ($S_{\text{BET}} = 79.09 \text{ m}^2 \cdot \text{g}^{-1}$). On the other hand, the Ce^{3+} doped matrix ($S_{\text{BET}} = 74.79 \text{ m}^2 \cdot \text{g}^{-1}$) showed a value very close to that of pure HAp, corroborating with the XRD data. Based on these data it is proposed that the Eu^{3+} and Gd^{3+} ions may also be occupying the interstices of the crystals of HAp or influencing the decrease of the unit cell as a function of their smaller rays.

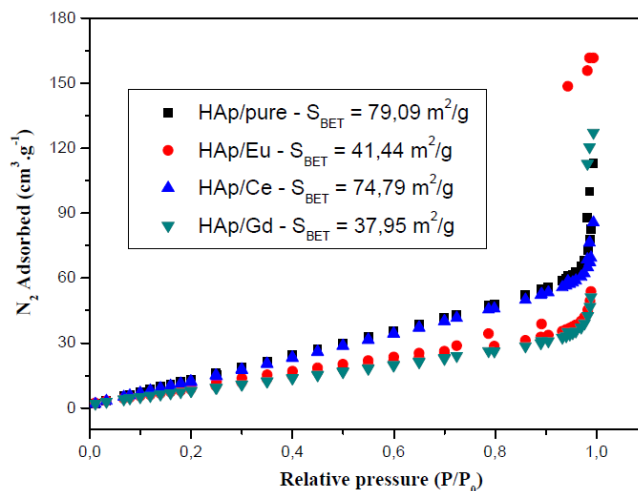


Figure 6: Nitrogen adsorption isotherms and BET surface area for pure HAp and doped with Eu^{3+} , Ce^{3+} and Gd^{3+} ions.

In Figure 7, the excitation and the emission spectra for the HAp are shown. The excitation spectrum (Figure 7-a) shows a broad band with two peaks at 310 nm and 350 nm ($\lambda_{\text{Em}} = 410$ nm). The emission spectrum ($\lambda_{\text{Ex}} = 350$ nm) shows a broad band with maximum 428 nm (Figure 7-b). In the work of ZHANG *et al.* [29], an emission with λ_{max} at 428 nm was also obtained for HAp microspheres, in this case, as Ca^{2+} ions or PO_4^{3-} groups are not able to generate photoluminescence, the study of the mechanism of the HAp synthesis indicated that the observed emission was attributed to the presence of impurities or defects in the host lattice of the material. Another possibility is that this emission originates from O-Ca charge transfer band.

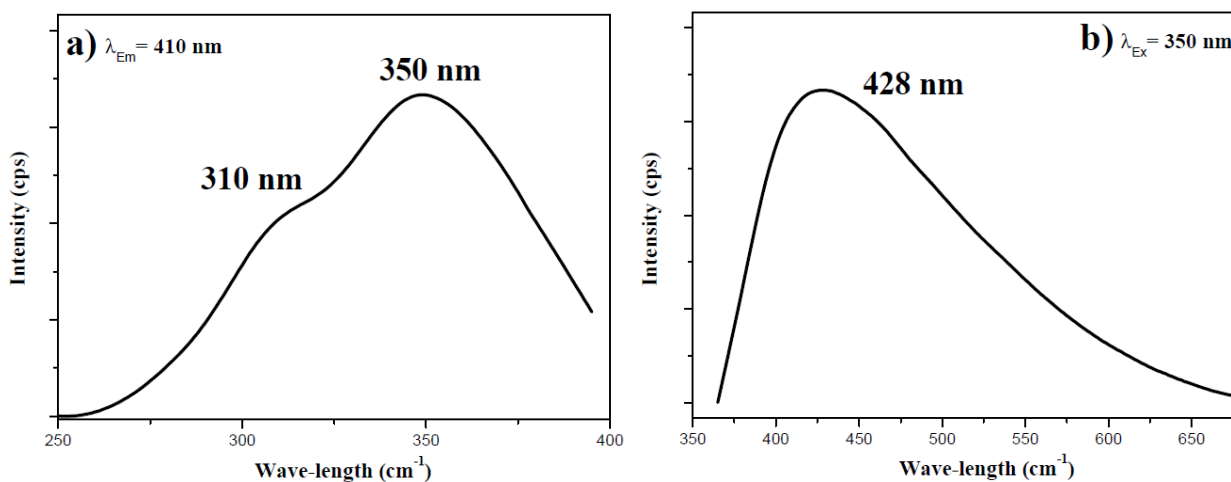


Figure 7: Spectra of a) excitation and b) emission for the matrix of Hap pure.

The HAp/Eu excitation spectra were obtained from emission monitoring at 611 nm ($^5\text{D}_0 \rightarrow ^7\text{F}_2$) and 573 nm ($^5\text{D}_0 \rightarrow \text{F}_0$), Figure 8-a. Both spectra present thin bands related to intraconfiguration transitions f-f. However, the excitation spectrum with emission monitoring at 573 nm exhibits a wide excitation band between 250 and 380 nm, attributed to a charge transfer transition between Eu^{3+} and O^{2-} [30]. Different excitation wavelengths were used to obtain the emission spectra of the HAp/Eu sample, Figure 8-b. In these, changes in the spectral profile are verified as a function of the excitation wavelength, indicating that it is possible to selectively excite Eu^{3+} ions with different symmetry sites, corroborating with the results of XRD and confirming the presence of more than one phase in the material and, consequently, different chemical environments. The emission spectra, with excitation at 335 nm, 522 nm and 565 nm, exhibit spectral profile with bands related to the transitions of the Eu^{3+} ion at: 573 nm ($^5\text{D}_0 \rightarrow \text{F}_0$), 600 nm ($^5\text{D}_0 \rightarrow \text{F}_1$), 622 and 628 nm ($^5\text{D}_0 \rightarrow \text{F}_2$). For the spectra obtained with excitation at 394 nm, 464 nm and 533 nm, the most intense emission bands were observed at: 611 nm ($^5\text{D}_0 \rightarrow \text{F}_2$) and 698 nm ($^5\text{D}_0 \rightarrow \text{F}_4$), in addition to less intense emissions at 573 nm, 577 nm, 617 nm, 622 nm and 628 nm [21, 31]. The presence of Eu^{3+} ions in two dis-

tinct environments in the host matrix can be explained by the existence of two different sites for the Ca^{2+} ions in the crystalline structure of HAp, called CaI and CaII (Figure 3). The CaI site has symmetry (C_3) and the CaII site, symmetry (Cs). According to MARTIM *et al.* [20] Eu^{3+} ions preferentially occupy the CaI site of HAp due to the better positioning to compensate for loads between the ions; however, the sample calcination process provides thermal energy for the system, inducing diffusion of the Eu^{3+} ions from the CaI site to the CaII site from 400 °C. The results agree with the migration mechanism of the ions through the matrix lattice, since the samples were calcined at 900 °C and the emissions obtained refer to the presence of Eu^{3+} ions simultaneously in the two different sites. The characteristic emission lines observed in the spectra show the potential for use of the material in applications linked to its photoluminescence monitoring, such as probe to investigate the degradation process of the material.

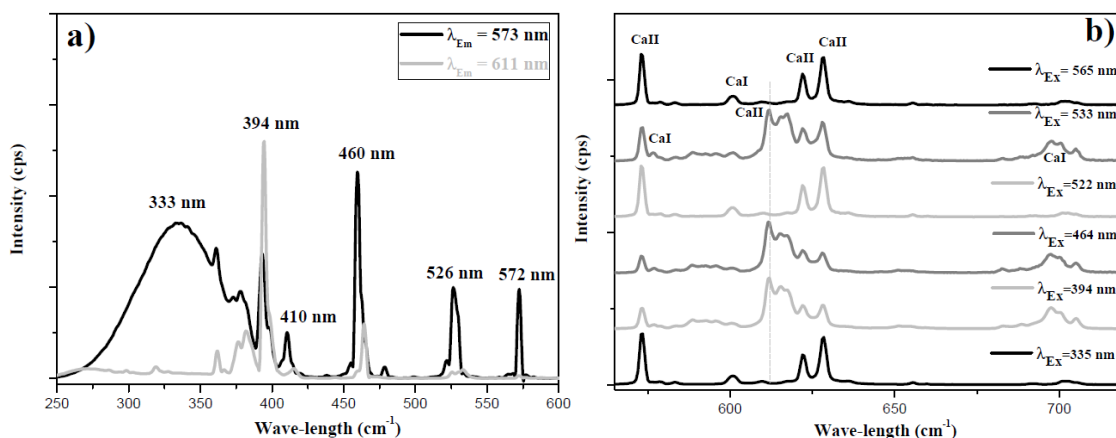


Figure 8: Spectra of a) excitation and b) emission of HAp doped with 2.0% Eu^{3+} ions.

For HAp/Ce, the excitation and emission spectra are shown in Figure 9. The excitation spectra ($\lambda_{\text{Em}} = 360 \text{ nm}$) exhibit three bands with maxima at 268, 295 and 315 nm. The emission spectrum shows two convoluted bands with maxima at 337 nm and 360 nm, Figure 9-b. Both the emission and excitation bands are attributed to interconfiguration transitions $5d \rightarrow 4f$ of the cerium ions. In the same way that ions Eu^{3+} , Ce^{3+} ions replace the two different Ca^{2+} sites in the HAp lattice, in agreement with the two emission peaks observed [32].

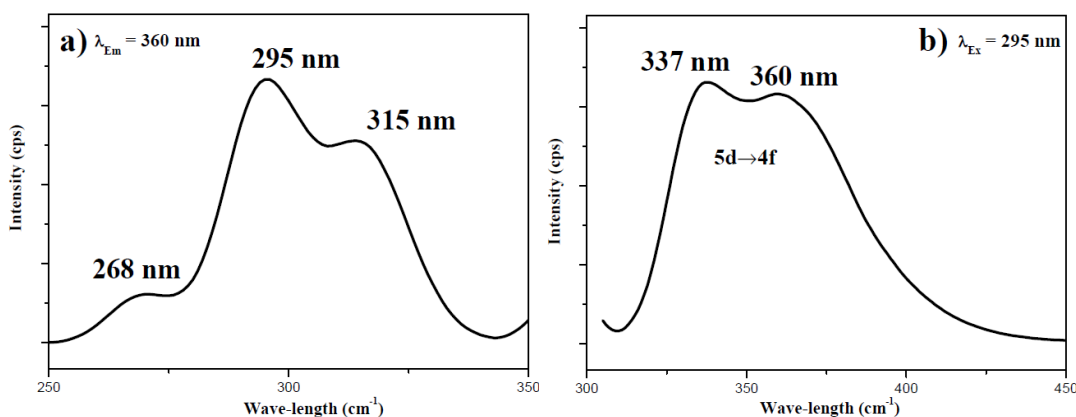


Figure 9: Spectra of a) excitation and b) emission of HAp doped with 2.0% Ce^{3+} ions.

The spectra for HAp/Gd are shown in Figure 10. The material was excited using the λ_{max} at 343 nm, Figure 10-a, for the acquisition of its emission spectrum shown in Figure 10-b, where it is observed a wide emission band at 425 nm. Since the energy difference between the ground state $^8S_{7/2}$ and the first excited state $^6P_{7/2}$ of the Gd^{3+} ion corresponds to the ultraviolet region [33] and the emission band observed for HAp/Gd appears in blue, this emission can be attributed to the matrix. On the other hand, it is known that gadolinium is a paramagnetic element widely used as a contrast agent in magnetic resonance diagnostics, so the incorporation of Gd^{3+} ions in HAp adds the image detection feature to the material [34].

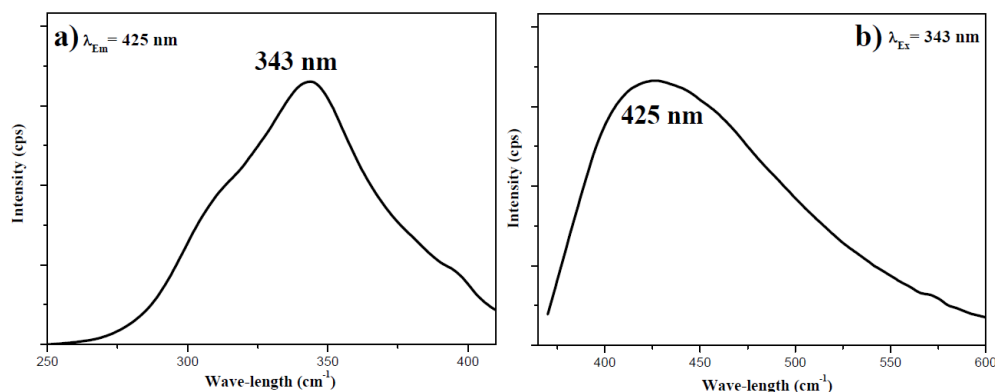


Figure 10: Spectra of a) excitation and b) emission of HAp doped with 2.0% Gd^{3+} ions.

4. CONCLUSION

In this work, the synthesis of hydroxyapatite doped with different lanthanide ions was presented. The results obtained from the characterizations showed the complete incorporation of Eu^{3+} and Gd^{3+} ions and partial Ce^{3+} ions into the crystalline structure of the matrix. The material doped with Eu^{3+} ions indicated a great photoluminescent potential, with intense emission peaks characteristic of the europium transitions. The HAp/Ce sample also demonstrated photoluminescence brought by the Ce^{3+} ions inserted into the HAp, while for HAp/Gd it was suggested photoluminescence attributed to the matrix. This research demonstrated that all the lanthanide ions studied had properties that allow the generation of images of the doped HAp, as well as the obtaining of a biphasic bioceramic HAp/TCP luminescent, making these materials good candidates for application as biosensors.

5. ACKNOWLEDGMENT

We acknowledge to Dr. Leonis L. da Luz for helpful in the photoluminescence data acquisition.

6. BIBLIOGRAPHY

- [1] HUGGES, J. M., RAKOVAN, J. "The Crystal Structure of Apatite, $Ca_5(PO_4)_3(F,OH,Cl)$ ". *Reviews in Mineralogy and Geochemistry*. <https://pubs.geoscienceworld.org/msa/rimg/article/48/1/1/110607/the-crystal-structure-of-apatite-ca5-po4-3-f-oh-cl>, v. 48 , n.1, pp. 1-12, 2002.
- [2] PAN, Y., FLEET, M. E. "Compositions of the Apatite-Group Minerals: Substitution Mechanisms and Controlling Factors". *Reviews in Mineralogy and Geochemistry*. <https://pubs.geoscienceworld.org/msa/rimg/article/48/1/13/110611/compositions-of-the-apatite-group-minerals>. v. 48 (2), pp. 13-49, 2002.
- [3] GOMES, D. S., SANTOS, A. M. C., NEVES, G. A., *et al.*, "A brief review on hydroxyapatite production and use in biomedicine", *Cerâmica*, <http://dx.doi.org/10.1590/0366-69132019653742706>, v. 65, pp. 282-302, 2019.
- [4] MAHDAVI, J. M.; KHAYATI, G. R. "Prediction of hydroxyapatite crystallite size prepared by sol-gel route: gene expression programming approach". *Journal of Sol-Gel Science and Technology*, <https://doi.org/10.1007/s10971-018-4601-6>, v. 86, pp. 112-125, 2018.
- [5] NAZEER, M. A., YILGOR, E., YAGCI, M. B., *et al.*, "Effect of reaction solvent on hydroxyapatite synthesis in sol-gel process". *R. Soc. open sci.* 4: 171098. <http://dx.doi.org/10.1098/rsos.171098>, 2017
- [6] MUBARAKALI, D. "Microwave irradiation mediated synthesis of needle-shaped hydroxyapatite nanoparticles as a flocculant for chlorella vulgaris". *Biocatalysis and Agricultural Biotechnology*, <https://doi.org/10.1016/j.bcab.2018.11.025>, v. 17, pp. 203-206, 2019.
- [7] ASRA, D. Y., SARI, Y. W., DAHLAN, K. "Effect of Microwave Irradiation on the Synthesis of Carbonated Hydroxyapatite (CHA) from Chicken Eggshell". *IOP Conf. Series: Earth and Environmental Science*, <https://doi.org/10.1088/1755-1315/187/1/012016>, v. 187, pp.012-016, 2018

- [8] LEE, I., LEE, J. A., LEE, J. H., HEO, Y. W., KIM, J. J. “Effects of pH and reaction temperature on hydroxyapatite powders synthesized by precipitation”. *Journal of the Korean Ceramic ty*, <https://doi.org/10.1007/s43207-019-00004-0>, v. 57, pp. 56–64, 2020.
- [9] AZEVEDO, A. G de S, STRECKER, K., GORGULHO, H. F. “Effect of temperature in process of sintering of hydroxyapatite powders”. *Cerâmica*. http://www.scielo.br/scielo.php?script=sci_arttext&pid=S0366-69132015000100008, v. 61, pp. 52-59, 2015.
- [10] REY, C., COMBES, C., DROUET, C., *et al.*, “Surface properties of biomimetic nanocrystalline apatites; applications in biomaterials”. *Progress in Crystal Growth and Characterization of Materials*, <http://dx.doi.org/10.1016/J.PCRYSGROW.2014.09.005>, v. 60, pp. 63-73, 2014.
- [11] POMPE, W., WORCH, H., HABRAKEN, W. J. M., *et al.*, “Octacalcium phosphate – a metastable mineral phase controls the evolution of scaffold forming proteins” *J. Mater. Chem. B*. <https://doi.org/10.1039/C5TB00673B>, v. 3, pp. 5318-5329, 2015.
- [12] ZENG, H., ZHANG, L., RONG, L., *et al.*, “A luminescent lanthanide coordination polymer based on energy transfer from metal to metal for hydrogen peroxide detection”. *International Journal of Biosensors & Bioelectronics*. <https://www.sciencedirect.com/science/article/pii/S0956566316311654>, v. 89, pp. 721-727, 2017.
- [13] CANTARELLI, I. X., PEDRONI, M., PICCINELLI, F., MARZOLA, P., BOSCHI, F., CONTI, G., *et al.* “Multifunctional nanoprobes based on up converting lanthanide doped CaF₂: towards biocompatible materials for biomedical imaging”. *Biomaterials. Sci*. <https://pubs.rsc.org/en/content/articlelanding/2014/bm/c4bm00119b#!divAbstract>, v. 2, 2014.
- [14] SOUZA, J. M., JÚNIOR, S. A., SÁ, G. F., AZEVEDO, W. M. “Doped polymers with Ln(III) complexes: simulation and control of light colors”. *Journal of Alloys and Compounds*. <https://www.sciencedirect.com/science/article/pii/S092583880200378X>, v. 344, pp. 320–322, 2002.
- [15] LIMA, P. P., MALTA, O. L., JÚNIOR, S. A. “Spectroscopic study of complexes of Eu³⁺, Tb³⁺ and Gd³⁺ with binders derived from dicarboxylic acids”. *Química Nova*. http://www.scielo.br/scielo.php?pid=S0100-40422005000500014&script=sci_abstract, v. 28(5), pp. 805-808, 2005.
- [16] BARBOSA, A. A., JÚNIOR, S. A., FERRAZ, A. V. “Study of a luminescent and antibacterial biomaterial based on hydroxyapatite as support for an antineoplastic drug”. *Journal of Materials Research*, <https://www.cambridge.org/core/journals/journal-of-materials-research/article/study-of-a-luminescent-and-antibacterial-biomaterial-based-on-hydroxyapatite-as-support-for-an-antineoplastic-drug/1249DF98088AECF269382D108D9348BA>, v. 34(11), pp. 1922–1930, 2019.
- [17] YANG, W. G., HA, J. H., KIM, S. G., *et al.*, “Spectroscopic determination of alkyl resorcinol concentration in hydroxyapatite composite”. *Journal of Analytical Science and Technology*. doi:10.1186/s40543-016-0089-2, v. 7, pp.1-5, 2016.
- [18] YANG, P., QUAN, Z., LI, C., KANG, X., *et al.*, “Bioactive, luminescent and mesoporous europium-doped hydroxyapatite as a drug carrier”. *Biomaterials*. <https://www.sciencedirect.com/science/article/pii/S0142961208005462>, v. 29, pp. 4341–4347, 2009.
- [19] CIOBANU, C. S., ICONARU, S. L., MASSUYEAU, F., *et al.*, PREDOI, D. “Synthesis, Structure, and Luminescent Properties of Europium-Doped Hydroxyapatite Nanocrystalline Powders”. *Journal Nanomaterials*. <https://www.hindawi.com/journals/jnm/2012/942801/>, v. 2012, pp. 1-9, 2012.
- [20] MARTIM, P., CARLOT, G., CHEVARIER, A., *et al.*, “Mechanisms involved in thermal diffusion of rare earth elements in apatite”. *Journal of Nuclear Materials*. <https://www.sciencedirect.com/science/article/pii/S0022311599001269>, v. 275(3), pp. 268–276, 1999.
- [21] SILVA, F. R. O., LIMA, N. B., GOUVEIA, D. S., *et al.*, Synthesis and characterization of Europium doped hydroxyapatite: Influence of excitation wavelength on Eu³⁺ luminescence in HA. *Material Science Forum*, <https://www.scientific.net/MSF.820.335>, v. 820, pp. 33-340, 2015.
- [22] HAN, Y., WANG, X., DAI, H., *et al.*, Synthesis and luminescence of Eu³⁺ doped hydroxyapatite nanocrystallines: Effects of calcinations and Eu³⁺ content. *Journal of Luminescence*. <https://www.sciencedirect.com/science/article/pii/S0022231312005704>, v.135, pp. 281–287, 2013.
- [23] LIN, K., CHANG, J. “Structure and properties of hydroxyapatite for biomedical applications. In: Hydroxyapatite (HAp) for Biomedical Applications”. 1th ed. eBook ISBN: 9781782420415.

<https://www.elsevier.com/books/hydroxyapatite-hap-for-biomedical-applications/mucalo/978-1-78242-033-0pp>. 3-19, 2015.

[24] ATINS, P. W., JONES, L. *Principles of chemistry: questioning modern life and the environmen*. 3ed. Porto Alegre: Bookman, 965 p., 2006.

[25] MORAIS, D. S., FERNANDES, S., GOMES, O. S., *et al.*, “Novel cerium doped glass-reinforced hydroxyapatite with antibacterial and osteoconductive properties for bone tissue regeneration”. *Biomedical Materials*. <https://www.ncbi.nlm.nih.gov/pubmed/26391473>, v.10(5), 2015.

[26] GYORGY, S., KAROLY, Z., FAZEKAS, P. *et al.*, “Efeito da temperatura da reação na morfologia da HAp nanosizada”. *J Therm Anal Calorim*, <https://doi.org/10.1007/s10973-019-08255-z>, v. 138, pp.145-151, 2019.

[27] KAMALANATHAN, P., RAMESH, S., BANG, L. T., *et al.*, “Synthesis and sintering of hydroxyapatite derived from eggshells as a calcium precursor”. *Ceramic International*. <https://www.sciencedirect.com/science/article/pii/S0272884214011080>, v. 40, pp. 16349-16359, 2014.

[28] SING, K. S. W., EVERETT, D. H., HAUL, R. A. W., *et al.*, “Reporting Physisorption Data for Gas/Solid Systems” In: *Pure and Applied Chemistry*. https://www.researchgate.net/publication/244739609_Reporting_Physisorption_Data_for_GasSolid_Systems_with_Special_Reference_to_the_Determination_of_Surface_Area_and_Porosity, v. 57(4), pp. 603-619, 1985.

[29] ZHANG, C., YANG, J., QUAN, Z., *et al.*, “Hydroxyapatite Nano- and Microcrystals with Multiform Morphologies: Controllable Synthesis and Luminescence Properties”. *Crystal Growth & Design*. <https://pubs.acs.org/doi/abs/10.1021/cg801353n>, v. 9(6), pp. 2725–2733, 2009.

[30] WANG, Y., GUO, X., ENDO, T., *et al.*, “Identification of charge transfer (CT) transition in (Gd,Y)BO₃:Eu phosphor under 100–300nm”. *Journal of Solid State Chemistry*. https://www.researchgate.net/publication/223602219_Identification_of_charge_transfer_CT_transition_in_GdYBO3Eu_phosphor_under_100-300nm, v. 177(7), pp. 2242-2248, 2004.

[31] HAN, Y., WANG, X. L. I. S. “Biocompatible Europium Doped Hydroxyapatite Nanoparticles as a Biological Fluorescent Probe”. *Current Nanoscience*. <http://www.eurekaselect.com/71370/article>, v. 6(2), pp. 178–183, 2010.

[32] CIOBANU, C. S., POPA, C. L., PREDOI, D. “Cerium-doped hydroxyapatite nanoparticles synthesized by the co-precipitation method”. *Journal of the Serbian Chemical Society*. https://www.researchgate.net/publication/290174295_Cerium_doped_hydroxyapatite_nanoparticles_synthesized_by_coprecipitation_method, v. 81(4), pp. 433–446, 2016.

[33] BRITO, H. F.,MALTA, O. L., FELINTO, M. C. F. C, *et al.*, “Luminescence phenomenon involving metal enolates”. *PATAI's Chemistry of Functional Groups*. <https://onlinelibrary.wiley.com/doi/10.1002/9780470682531.pat0419>, 2010.

[34] CIPRESTE, M. F., PERES, A. M., COTTA, A. A. C., *et al.*, “Synthesis and characterization of 159Gd-doped hydroxyapatite nanorods for bioapplications as theranostic systems”. *Materials Chemistry and Physics*. <https://www.sciencedirect.com/science/article/pii/S0254058416304771>, v. 181, pp. 301-311, 2016.

ORCID

Amanda Alves Barbosa	https://orcid.org/0000-0003-0266-4604
Severino Alves Junior	https://orcid.org/0000-0002-8092-4224
Raquel Aline Pessoa Oliveira	https://orcid.org/0000-0002-8455-1226
Andréa de Vasconcelos Ferraz	https://orcid.org/0000-0001-8043-1414